Geomechanics and Engineering, *Vol. 35, No. 6 (2023) 603-615*
https://doi.org/10.12989/gae.2023.35.6.603

The responses of battered pile to tunnelling at different depths relative to the pile length

Mukhtiar Ali Soomro[1], Naeem Mangi*[2], Dildar Ali Mangnejo[3] and Zongyu Zhang[2]

[1]*School of Mechanics and Civil Engineering, China University of Mining and Technology, Xuzhou, Jiangsu, P.R. China*
[2]*School of Civil Engineering, Southwest Jiaotong University, Chengdu 610031, China*
[3]*Department of Civil Engineering, Mehran University of Engineering and Technology, Shaheed Zulfiqar Ali Bhutto Campus, Khairpur Mir's, Sindh, Pakistan*

(*Received September 26, 2023, Revised November 7, 2023, Accepted November 23, 2023*)

Abstract. Population growth and urbanization prompted engineers to propose more sophisticated and efficient transportation methods, such as underground transit systems. However, due to limited urban space, it is necessary to construct these tunnels in close proximity to existing infrastructure like high-rise buildings and bridges. Battered piles have been widely used for their higher stiffness and bearing capacity compared to vertical piles, making them effective in resisting lateral loads from winds, soil pressures, and impacts. Considerable prior research has been concerned with understanding the vertical pile response to tunnel excavation. However, the three-dimensional effects of tunnelling on adjacent battered piled foundations are still not investigated. This study investigates the response of a single battered pile to tunnelling at three critical depths along the pile: near the pile shaft (S), next to the pile (T), and below the pile toe (B). An advanced hypoplastic model capable of capturing small strain stiffness is used to simulate clay behaviour. The computed results reveal that settlement and load transfer mechanisms along the battered pile, resulting from tunnelling, depend significantly on the tunnel's location relative the length of the pile. The largest settlement of the battered pile occurs in the case of T. Conversely, the greatest pile head deflection is caused by tunnelling near the pile shaft. The battered pile experiences "dragload" due to negative skin friction mobilization resulting from tunnel excavation in the case of S. The battered pile is susceptible to induced bending moments when tunnelling occurs near the pile shaft S whereas the magnitude of induced bending moment is minimal in the case of B.

Keywords: battered pile; bending moment; settlement; stiff clay; tunnelling

1. Introduction

Population growth and space limitations have pushed engineers to propose more sophisticated and efficient means of transportation (Ding *et al.* 2017). As a result, underground transit systems have gained more attention (Liu *et al.* 2023, Ye *et al.* 2023, Shi *et al.* 2019a, 2023). However, due to the scarcity of urban space, it is inevitable to construct these tunnels in close proximity to existing infrastructures such as high-rise building, bridges (Lu *et al.* 2020, Lee 2019). Battered piles have been used for a long time to resist large lateral loads from winds, water waves, soil pressures, and impacts (Bharathi *et al.* 2022, Mu *et al.* 2021). Their distinct advantage over vertical piles is that they transmit the applied lateral loads partly in axial compression, rather than only through shear and bending. However, given the limited urban space, it is unavoidable to construct these tunnels near existing infrastructures which can cause additional settlement, lateral movement and tilting of piled structure which may jeopardize the piled foundation (Soomro *et al.* 2022). Jacobsz *et al.* (2006) reported the 35-km long twin tunnels were constructed adjacent to a bridge supported by vertical and battered pile. Each bridge pier is supported on a total of 31 piles of which 12 are vertical and 19 battered. The vertical piles were of driven-cast-in situ construction, while the battered piles were bored. Hence, it is crucial to investigate the impact of tunnelling on adjacent battered piles. Extensive research has been conducted to investigate the effects of single tunnels as well as twin tunnels effects on vertical piles. Various scholars have documented case histories that illustrate instances of excessive settlement and lateral deflection of piles induced by tunnelling (Forth and Thorley in 1996, Coutts and Wang 2000, Pang *et al.* 2005, Selemetas 2005, Jacobsz *et al.*2006; Boonyarak *et al.* 2014). Moreover, researchers have conducted physical model tests to examine the behaviour of piles in response to single tunnel excavations (Loganathan *et al.* 2000, Lee and Chiang 2007, Marshall and Mair 2011, Franza and Marshall 2018, Meguid *et al.* in 2008, and Boonsiri and Takemura in 2015). These investigations have demonstrated that the extent of tunnelling-induced settlements is significantly influenced by factors such as tunnel volume loss and the depth at which the tunnel is buried relative to the piles. Franza and Marshall (2018) carried out a set of centrifuge experiments with the aim of simulating the impact of tunnel excavation beneath piled structures in dry sand. The findings of their research demonstrate that the settlement and failure mechanisms of the piles are greatly influenced by the initial loads on the piles and the redistribution of these loads

*Corresponding author, Ph.D. candidate
E-mail: naeem08ce30@gmail.com

ISSN: 2005-307X (Print), 2092-6219 (Online)

Table 1 Summary of numerical simulations

Case ID	C/D	Remarks
S	1.33	Tunnelling near pile shaft and opposite side of batter pile
T	2.33	Tunnelling next to pile toe and opposite side of batter pile
B	3.53	Tunnelling below pile toe and opposite side of batter pile

Note: *C/D*= cover to diameter of tunnel ratio

among the piles during the loss of tunnel volume. These factors are directly associated with the weight and stiffness of the structures. Furthermore, several researchers (Loganathan *et al*. 2001, Mroueh and Shahrour 2002, Lee and Ng 2005, Huang *et al*. 2009, Zhang *et al.* 2011, Marshall 2012, Lee 2012a, Lee 2012b, Lee 2013, Hong *et al*. 2015, Soomro *et al.* 2015, Soomro *et al.* 2017) have investigated this issue by proposing analytical solutions and conducting numerical modelling. In order to further explore the effects of twin tunnelling on both individual piles and pile groups in dry sand, centrifuge model tests were conducted, and subsequent analysis was performed (Ng and Lu 2013, Ng *et al.* 2013, Ng *et al.* 2014, Ng *et al.* 2015). These tests simulated side-by-side twin tunnels either adjacent to or beneath the toe of the piles. The existing single pile or pile group was situated between the twin tunnels, which were excavated sequentially. The results revealed that twin tunnelling did not induce significant bending moments in either case, with the induced moment not exceeding 17% of the pile's bending moment capacity. Additionally, twin tunnelling caused a maximum increase in axial force of 27% in the single pile due to load transfer within the pile. Furthermore, the second tunnelling process reversed the tilting effect on the existing pile group caused by the first tunnelling. Considerable prior research has been concerned with understanding the vertical pile response to tunnel excavation. However, the three-dimensional effects of tunnelling on adjacent battered piled foundations are still not investigated.

In view of the aforementioned issues, this study aims at systematically investigating the settlement and load transfer mechanism of an existing battered single pile due to tunnel in saturated clay. To achieve these objectives, a three-dimensional coupled-consolidation numerical parametric study is carried in this study. Settlement and deflection of the battered pile, py curves, axial load distribution along the pile, stress changes and bending moment during tunnelling advancement are reported and discussed.

2. Development of three-dimensional numerical model

2.1 Description of geometry of the numerical models

The present study investigates the effects of an advancing tunnel on an existing battered pile in medium stiff clay. To achieve this, numerical analyses are conducted using the three-dimensional finite element program Abaqus 6.14-2 (Hibbitt *et al.* 2015). The analysis takes into account the soil consolidation that occurs during tunnel construction through the implementation of coupled-consolidation analysis. The study investigates the depth of the tunnel in relation to the length of the pile. Three critical depths along the pile depths are selected which are near the pile shaft (S), next to (T) and below the pile toe (B) considering the position of the tunnel on the opposite side of battered pile.

The cases are denoted according to tunnel location relative to pile length e.g., S represents the case in which tunnel is excavated near the pile shaft on the opposite side of the battered pile. Figs. 1(a)-1(c) illustrate the elevation view of cases S , T, and B, respectively. In the case of S, the tunnelling is simulated near the adjacent pile shaft on the opposite side of the pile batter. Conversely, in the T and B cases, the tunnel is excavated next to pile toe and below the pile toe, respectively. The tunnel diameter is taken as 6 m (D) with a cover of 8 m (C), resulting in a cover-to-diameter ratio (C/D) of the tunnel equal to 1.33 in case of S. For the cases of T and B, a cover-to-diameter ratio (C/D) of the tunnel equal to 2.33 and 3.53, respectively. The embedded length (L_p) and diameter (d_p) of the pile are 18 m and 0.8 m, respectively. The pile is inclined at a batter angle (θ) of 20°, which is the optimized angle for the battered pile (Bharathi *et al*. 2022, Jamil and Ahmed 2019). A working load in vertical direction is applied on the battered pile head. The magnitude of the vertical working load is determined from a pile load test which is conducted numerically (discussed in section 2.4). The clear distance (s) between the tunnel and the battered pile is 2.5 m, equivalent to 0.42D.

Fig. 2 illustrates the plan view of the configuration of the numerical simulation. The tunnel in the simulation has a length of 72 m, which corresponds to 12 times the diameter (D) of the tunnel. The excavation process of each tunnel was simulated in 28 steps. During each step, the tunnel advanced by a distance of 2.5 m (0.42D) (Lee 2012, Lee and Ng 2005). In the finite element analysis, a time increment of one day was used for each step. To monitor the progress of the tunnel advancements, a monitoring section located at the transverse centreline of the pile (i.e., y/D = 0) was selected as a reference point.

The primary objective of this study is to examine the effects of tunnelling on a battered pile under vertical working load. To achieve this, a numerical pile load test (L) is conducted in "greenfield" conditions, meaning no tunnels are present. The purpose of this test is to determine the ultimate capacity of the pile in medium stiff clay. After the ultimate capacity is determined from the pile load test, the working load is calculated by applying a factor of safety of 3.0 (Polous 2001). This ensures a sufficient margin of safety in the design (Lu *et al.* 2020, Shi *et al.* 2020, Qian *et*

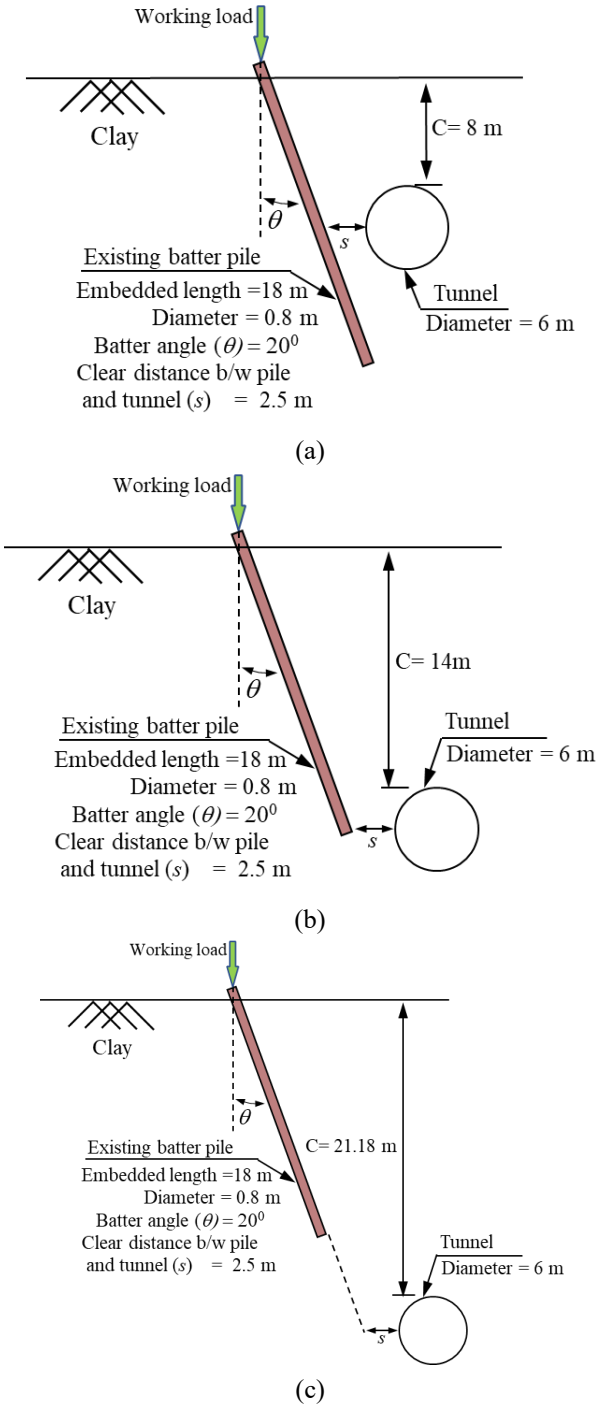

Fig. 1 Elevation view of numerical simulations of cases (a) S, (b) T and (c) B

al. 2020). The obtained working load is then applied to the battered pile in the subsequent numerical simulations. Table 1 summarizes numerical simulations conducted in this study.

2.2 Geometry discretisation, boundary and initial conditions

The 3D FE simulations discussed in the paper aimed to model the battered pile responses to an adjacent advancing tunnel. Fig. 3 shows an isometric view of a typical finite element mesh of the case T_b. The length along the y-axis, width along the x-axis, and depth along the z-axis of the mesh are 80 m, 80 m, and 60 m, respectively. The depth of the model is chosen to be 10 time the diameter of the tunnel. The mesh consists of 88752 elements and 100145 nodes. The soil domain is discretized using 8-node brick, trilinear displacement, trilinear pore pressure. Coupled-consolidation analysis was performed to simulate accumulation of excess pore water pressure. The pile is discretized using 8-node linear brick. The sensitivity of the numerical results with respect to size of mesh was explored

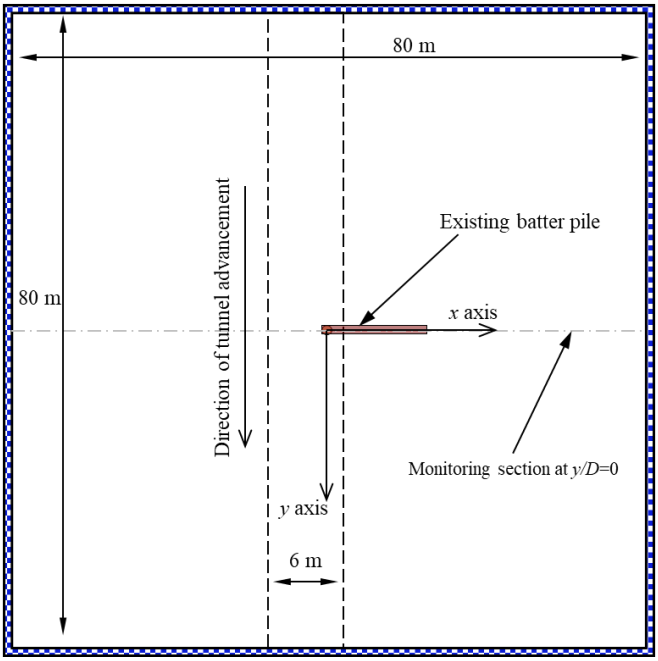

Fig. 2 Plan view numerical simulation of a typical case of S

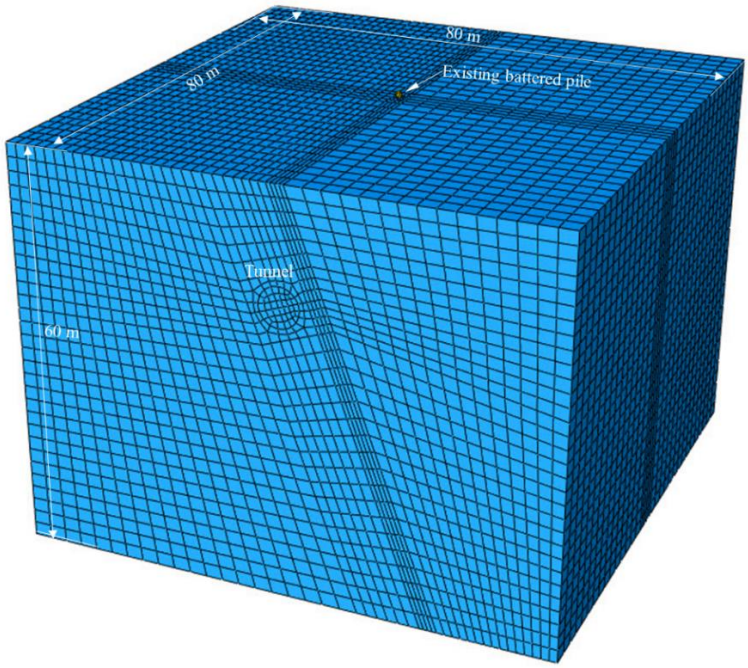

Fig. 3 Finite element mesh of a typical numerical analysis for the case of T

and it was found that without undermining stability of analysis, the optimum value 1.5 mm of element was chosen. All displacement components were prescribed to be zero at the base of the mesh, while only displacements orthogonal to the boundaries were restrained on the vertical sides. The effective vertical stress was initialized in the numerical model by adopting a saturated bulk unit weight of 16.5 kN/m^3 and the hydrostatic pore pressure distribution. The coefficient of lateral earth pressure at rest, Ko is estimated by Mayne and Kulhawy's equation $\left(\text{i.e.}, K_0 = (1 - sin\varphi')(OCR)^{sin\varphi'}\right)$.

In order to consider the interaction between soil and structures, specific properties related to tangential behaviour and normal behaviour are chosen for the contact between the battered piles nd soil. The Coulomb Friction model is utilized to define frictional contact properties, enabling the simulation of tangential behaviour. On the other hand, the Hard Contact model is employed to replicate the nature of surface contact and simulate normal behaviour in Abaqus. In all analyses, a standard value of μ (coefficient of friction) for a bored pile was assumed to be 0.35 (Indraratna *et al*. 1992, Tsubakihara and Kishida 1993,

Karira *et al.* 2022). To achieve complete mobilization of the interface friction, a limiting shear displacement of 5 mm is considered, corresponding to μ multiplied by *p*', where *p*' represents the normal effective stress between the two contact surfaces. This approach is implemented consistently throughout the analyses.

In this study, the displacement-controlled model (DCM) was utilized, following the approach proposed by Cheng *et al.* 2007. Prior to the tunnelling process, the volume loss was predetermined by defining the dimensions of the gap between the tunnel lining and the excavated soil. The soil in this specific section was removed by employing a technique referred to as "element death". Simultaneously, the shell element representing the tunnel lining was activated. Mair and Taylor (1997) documented that tunnel excavation using earth pressure balance shields resulted in typical volume losses of up to 1% in sand, while soft clay exhibited volume losses of approximately 2%. Additionally, Abrams (2007) and Shirlaw *et al.* (2003) reported volume losses ranging from 1% to 4% in mixed-face tunnelling scenarios involving clay and sand. Based on these reports, a volume loss of 2% was adopted in this hypothesized study.

2.3 Material models and input parameters

A hypoplastic(clay) model is used to capture behaviour of soil which is capable to model small strain stiffness (Mašin 2005). The basic hypoplastic model was developed to capture the nonlinear behaviour of granular materials under medium-to-large strain levels during monotonic loading (Mašín and Herle 2005, Mašín 2005). This model consists of five parameters, namely $N, \lambda^*, \kappa^*, \varphi_c$ and r. The parameters N and λ^* define the position and slope of the isotropic normal compression line in the ln(1+e) versus ln(p') plane, where e represents the void ratio and *p'* denotes the mean effective stress. The parameter κ^* defines the slope of the isotropic unloading line in the same plane. φ_c represents the critical state friction angle, while r controls the shear modulus at large strains. To incorporate strain dependency and path dependency of soil stiffness at small strains, Niemunis and Herle (1997) improved the basic hypoplastic model by introducing the concept of intergranular strain. This enhancement requires five additional parameters: $(R,\ \beta_r,\ \chi,\ m_T\ and\ m_{R,})$. The parameter R determines the size of the elastic range, while β_r and χ control the rate at which stiffness degrades. The parameters $m_T\ and\ m_R$ govern the initial shear modulus when the strain path is reversed by 180° and 90°, respectively. The hypoplastic clay model, including small strain stiffness, has been implemented in the commercial finite element software package Abaqus as a user-defined subroutine.

In this hypothetical study, kaolin clay was selected as the artificial soil due to its extensively studied physical properties and basic geotechnical parameters. The choice of kaolin clay is supported by prior research that has focused on microstructure characterization (Gasparre 2005), seepage tests (Al-Tabba 1987), compression tests, and shear tests (Benz 2007). Additionally, kaolin clay has been widely used as a standard testing material for model tests that simulate different soil-pile interaction problems (Loganathan *et al.* 2000, Wang *et al.* 2015). The parameters for the hypoplastic clay model used in this study are adopted from previous research (Soomro *et al.* 2020). The researchers calibrated these parameters by comparing them against experimental results reported in the literature. Furthermore, they validated their parameters by comparing them with the measured results of cyclic behaviour of piles in centrifuge tests. Four out of the 10 parameters for kaolin clay have been widely studied and reported (i.e., N, λ^*, κ^* and φ_c). Based on these four known parameters, the other six model parameters controlling soil stiffness at medium to large-strain levels (i.e., r) and at small-strain levels (i.e., $R,\ \beta_r,\ \chi,\ m_T\ and\ m_R$) were calibrated against existing experimental data of kaolin clay. The model parameters at small-strain and large-strain ranges are calibrated against the measured stress–strain relationships (reported by Parry and Nadarajah 1974) and the measured stiffness degradation curves (reported by Benz 2007) in kaolin clay, respectively. All model parameters for clay and concrete are summarized in Table 2 and Table 3, respectively.

2.4 Determination of working load for the pile

In this parametric study, the primary objective is to investigate the battered pile responses when subjected to a working load during the advancement of tunnel in clay. To determine the ultimate load carrying capacity of the battered pile (and hence the working load), a computed load-settlement relationship was obtained from simulation L as shown in Fig. 4. The load applied on the pile was gradually increased to 4 MN over a period of 24 h. Based on the failure criterion, suggested by ISSMFE (1985) (i.e., 10% of pile diameter), the ultimate bearing capacity of 3.2 MN was computed. Using factor of safety as 3, the working load was determined to be 1067 kN. The settlement of the battered pile is computed as 12.0 mm (1.5% d_p) due to application of the vertical working load.

3. Interpretation of computed results

3.1 Progressive pile settlement due to advancement of tunnelling

Fig. 5 compares the induced settlement of the battered pile during construction of tunnel in cases of S, T and B. The induced settlement (S_p) is expressed as percentage of the pile diameter (d_p). The passage of the tunnel is represented by normalized distance by tunnel diameter (*y/D*) which is measured from monitoring section. It can be seen from the figure that no settlement is induced when the tunnel is sufficiently far from the pile (i.e., at the monitoring section where *y/D*=0) in all three cases. However, as the tunnel face reaches a distance of *y/D*=-4.0 behind the pile, the battered pile begins to experience settlement. The induced settlement further increases as tunnelling activity is carried out closer to the pile.

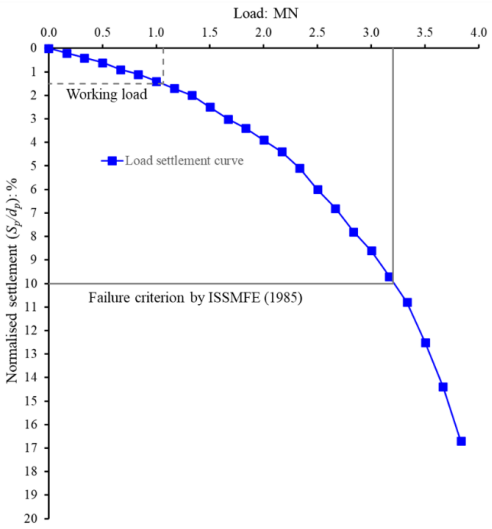

Fig. 4 Load settlement curve obtained from the load test

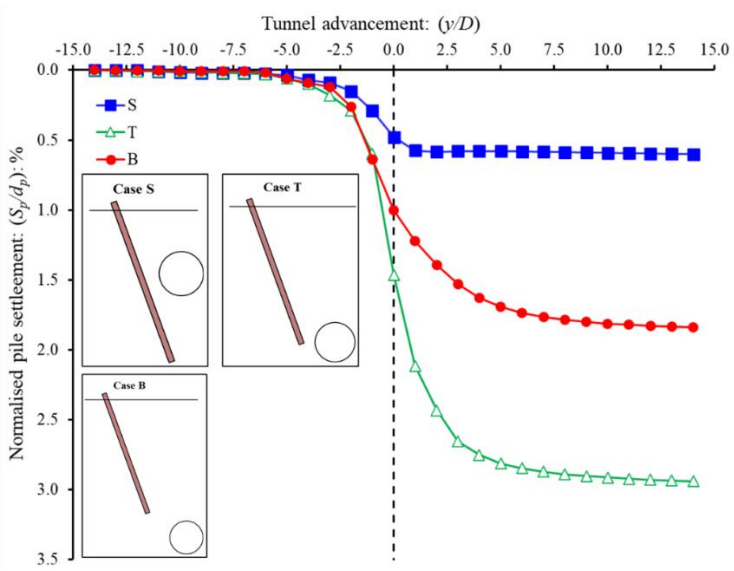

Fig. 5 Induced settlement of battered pile during tunnelling in cases of S, T and B

Table 2 Model parameters of kaolin clay adopted in the parametric study

Description	Parameter
Effective angle of shearing resistance at critical state: ϕ'	22°
Parameter controlling the slope of the isotropic normal compression line in the ln(1 + e) versus lnp plane, λ^*	0.11
Parameter controlling the slope of the isotropic normal compression line in the ln(1 + e) versus lnp plane, κ^*	0.026
Parameter controlling the position of the isotropic normal compression line in the ln(1 +e)– lnp plane, N	1.36
Parameter controlling the shear stiffness at medium- to large- strain levels, r	0.65
Parameter controlling initial shear modulus upon 180° strain path reversal, m_R	14
Parameter controlling initial shear modulus upon 90° strain path reversal, m_T	11
Size of elastic range, R	1×10^{-5}
Parameter controlling the rate of degradation of the stiffness with strain β_r	0.1
Parameter controlling degradation rate of stiffness with strain χ	0.7
Initial void ratio, e	1.05
Dry density (kg/m^3)	1136
Coefficient of permeability, k (m/s)	1×10^{-9}

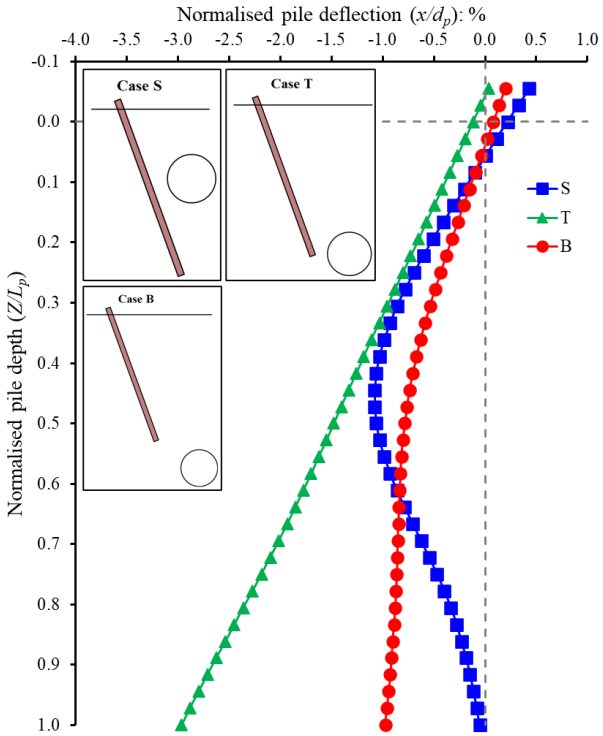

Fig. 6 Induced pile deflection on completion of tunnel

Table 3 Concrete parameters adopted in finite element analysis

Description	Parameter
Young's Modulus, E	35 GPa
Poisson's ratio, ν	0.3
Density, ρ	2400 kg/m^3

However, no substantial settlement was observed when the tunnelling activity is carried out at a distance of y/D=+4.0 both in front of and beyond the pile. Thus, the zone of influence was identified as being between y/D=-4.0 and y/D=+4.0. Furthermore, the maximum settlement was induced in the battered pile when the tunnel was excavated on opposite side of the battered pile in case of T. This observation is different from that was made when tunnel passes near the pile shaft. This is because the lower part of the pile including the pile toe is substantially affected by the stress relief due to tunnelling next to the pile toe in case of T (discussed in section 3.5). For case of B, the settlement of the battered pile is attributable to reduce mobilized end-bearing of the pile (discussed in section 3.4) due to tunnelling-induced stress release (discussed in section 3.5). The battered pile has to settle in order to mobilize shaft resistance. The final induced settlement of 0.60%d_p, 2.94%d_p and 1.84%d_p computed in cases of S, T and B, respectively.

In case of tunnelling excavated near the pile shaft (i.e., case S), negative deflection was induced in the battered pile (with a maximum of 1.07%d_p at Z/L_p=0.44), and negligible movement was induced at the pile head. This occurred because the location of the tunnel (relative to the batter side of the pile) was opposite to the batter side of the pile in the case of S. The ground movement due to tunnelling (discussed in section 3.3) dragged the battered pile towards the tunnel, but the normal components to the battered pile pulled the pile in the opposite direction to the drag caused by tunnelling. The tunnel excavation in case of T induced lateral movement as rigid body movement (with maximum values of -3.0%d_p) at the pile toe. This mechanism can be attributed to push from the tunnelling-induced ground movement as well as the normal component of the vertical working load applied on the pile head. In contrast to intuition, the maximum lateral movement (with maximum values of -1.0%d_p) in the toe of the battered pile is induced in case of B. This is because of the coupled effects of ground movement due to tunnelling-induced stress release (discussed in section 3.5) and the normal component of the vertical working load on the pile head. The normal component of the pile caused lateral movement of the upper portion of the pile and the ground movement drag the pile toe towards tunnel in case of B. The deflection of -2.96%d_p and -0.97%d_p were induced at the pile toe due to tunnelling in cases of T and B, respectively.

3.2 Induced lateral movement of pile due to tunnelling

Fig. 6 shows deflection of the battered pile on completion of tunnelling near pile shaft in cases of S, T and B. The positive value represents lateral movement of the pile towards the tunnel.

In case of tunnelling excavated near the pile shaft (i.e., case S), negative deflection was induced in the battered pile (with a maximum of 1.07%d_p at Z/L_p=0.44), and negligible movement was induced at the pile head. This occurred because the location of the tunnel (relative to the batter side

of the pile) was opposite to the batter side of the pile in the case of S. The ground movement due to tunnelling (discussed in section 3.3) dragged the battered pile towards the tunnel, but the normal components to the battered pile pulled the pile in the opposite direction to the drag caused by tunnelling. The tunnel excavation in case of T induced lateral movement as rigid body movement (with maximum values of -3.0%d_p) at the pile toe. This mechanism can be attributed to push from the tunnelling-induced ground movement as well as the normal component of the vertical working load applied on the pile head. In contrast to intuition, the maximum lateral movement (with maximum values of -1.0%d_p) in the toe of the battered pile is induced in case of B. This is because of the coupled effects of ground movement due to tunnelling-induced stress release (discussed in section 3.5) and the normal component of the vertical working load on the pile head. The normal component of the pile caused lateral movement of the upper portion of the pile and the ground movement drag the pile toe towards tunnel in case of B. The deflection of -2.96%d_p and -0.97%d_p were induced at the pile toe due to tunnelling in cases of T and B, respectively.

3.3 Tunnelling induced displacement and shear strain mechanisms

To understand the mechanisms of tunnelling-induced soil movement and shear strain generated in the ground and its effects on the battered pile, displacement vectors and shear strain contours were drawn from selected elements at the monitoring section (i.e., y=0) for all the cases. Figs. 7(a), (b) and (c) show the tunnelling-induced displacement vectors and shear strains in cases of S, T, and B, respectively. It can be seen that the induced ground movement due to tunnel excavated near the battered pile shaft is towards the tunnel in all cases. This is because of tunnelling induced stress release due to 2% of volume loss. As result of this, significant shear strains were generated around the tunnel.

In case of S (in which tunnel is excavated on the other side of the tunnel), the shear strains were induced underneath the pile toe. This is because of mobilization of the end-bearing of the pile due to reduction in shaft resistance and "dragload" resulting from negative skin friction. As a consequence of this, the induced settlement of the battered pile in case of S occurred (see Fig. 5). On the other hand, both the tunnelling-induced ground movement and intensive shear strain around the pile toe, and the action of normal component of vertical working load in case of T, caused larger settlement (see Fig. 5) and lateral movement (see Fig. 6) in the pile toe than that in case of S. It can be seen that the displacement vectors near the tunnel are larger than that near the ground surface in case of B. Since the tunnel is excavated below the pile toe, the tunnelling-induced stress release caused reduction of the end-bearing of the battered pile (discussed in section 3.5). The pile had to settle to mobilise the shaft resistance of the pile (see Fig. 5). The counter-intuitive settlement behaviour is because of the ground movement towards the tunnel drag the pile in case of B. The settlement of the battered pile led to generate

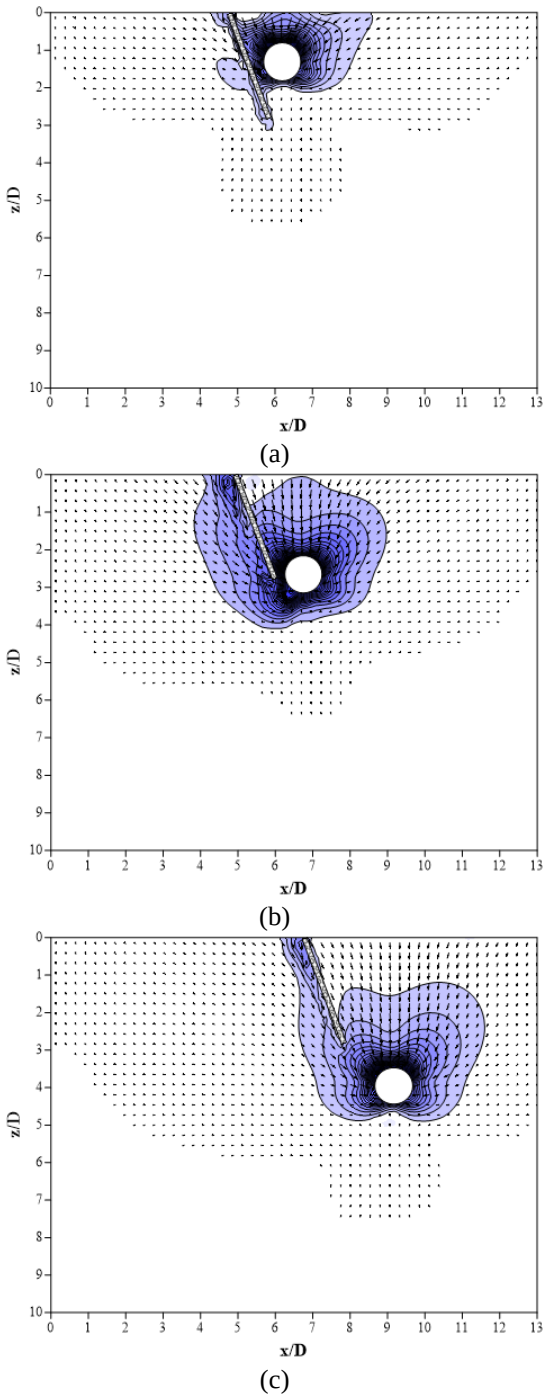

Fig. 7 Displacement vectors and shear strain contours around the pile due to tunnelling in cases of (a) S, (b) T and (c) B

substantial shear strains on the battered side of the pile. Therefore, the induced pile deflection at the toe of the pile (see Fig. 6).

3.4 Changes in load distribution along the length of the pile

As discussed in previous section, the vertical working load applied on the battered pile head is resolved into two components (i.e., one normal to the pile and the other in the

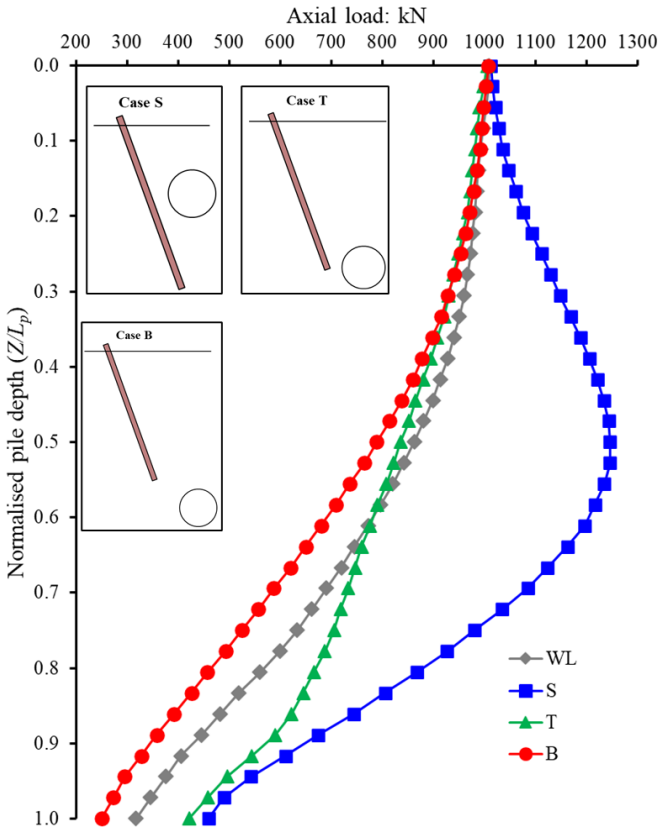

Fig. 8 Changes in axial load along the pile length near pile shaft; next to the pile toe; and below the pile toe

axial direction.). In this section changes in load in axial direction along the length of the battered pile due to tunnelling is explored. Fig. 8 compares the axial load distribution along the battered pile before (but after application of the working load) and after the tunnelling in cases of S, T and B. The axial component (i.e., 1010 kN) of the vertical working load (i.e., 1070 kN) was carried is carried by the battered pile through a combination of 70% with shaft resistance and remainder 30% with end-bearing of the pile.

In cases of S, the upper half portion of the battered pile is subjected to the "dragload" due to negative skin friction mobilization on completion of tunnel. However, shaft resistance along the upper portion vertical pile (i.e., Z/Lp<0.42) decreases to zero. This is because of the battered pile shaft is subjected to stress release due to tunnelling (discussed in section 3.5). Since the battered piles are installed at an inclination, the soil settled larger than the pile resulting in pulling the battered pile downward which cause negative shaft resistance along the battered pile. In order to ensure the pile maintained its equilibrium, positive skin friction (PSF) along the lower portion of the pile at the interface between the pile and the soil, as well as end-bearing resistance are mobilized. On completion of tunnel, mobilized shaft resistance and the end-bearing increased to 9% and 28% in case of S, respectively. Due to tunnelling next to the pile toe in case of T, the resistance along the lower portion of the pile is decreased due to stress release induced by tunnelling (as discussed in section 3.5). To compensate for the reduction in shaft resistance, the settlement of the pile (as shown in Fig. 5) mobilizes both the shaft resistance and the end-bearing of the pile. Therefore, the largest settlement occurs due to tunnelling in the case of T. In contrast, the axial load decreased along the entire length of the battered pile in case of B. This is because of the tunnel led to reductions in the end-bearing of the pile as a result of stress release. To compensate for the decrease in end-bearing resistance, the pile has to settle substantially (see Fig. 5) to mobilise the shaft resistance along the entire pile length. The end-bearing is decreased by 21% and the shaft resistance is increased by 10% due to tunnelling.

3.5 Changes in normal stress on the piles

The load transfer along a pile can be attributed to several factors, including the normal stresses acting on the pile shaft, the angle of friction between the soil and the pile interface, and the degree of relative displacement between the pile and the surrounding soil. To understand the normal stress changes on the pile, elements at the monitoring section are selected to draw stress contours. Figs. 9(a)-9(c) illustrate the contours of stress changes in the selected elements in cases of S, T and B, respectively. The purple and red colored contour lines represent increases and reductions in stresses, respectively. The phenomenon of soil arching causes a decrease in horizontal effective stresses at the springline of the tunnels, while an increase in stress levels is observed at the tunnel crown and invert (Jacobsz 2004, Ng and Lee 2005). Since tunnel is located adjacent to

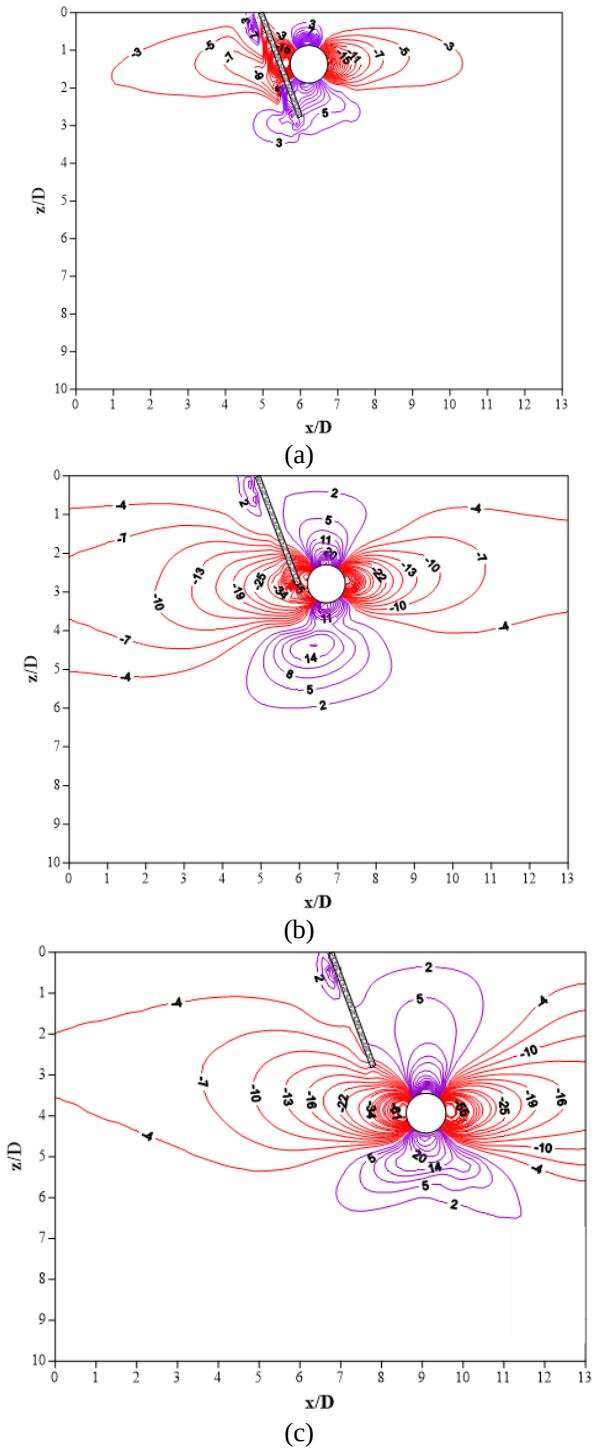

Fig. 9 Changes in stresses contours around the pile due to tunnelling in cases of (a) S (b) T and (c) B

the pile shaft in case of S, the pile shaft is subjected to the stress release and stress increment at the pile toe. This led to negative shaft resistance along the battered pile (see Fig. 8). Because the location of the tunnel is next to the pile toe in case of T, the stress release resulting from the tunnel affects both the lower part of the pile shaft and the pile toe. Slight increase in stress is induced under the left side of the upper portion of the pile in case of T. This is because of the tunnel location is on the other side of the batter of the pile. As a result, the largest settlement is induced in the battered pile in case of T. On the other hand, in case of B, the pile toe experiences the stress reduction due to tunnelling. As a result, end-bearing of the pile decreases, and shaft resistance is mobilized along the pile length (see Fig. 8).

3.6 Induced bending moment along the length of the pile

As discussed in section 3.4, the vertical working load applied to the head of the battered pile is resolved into two components. One component acts normal to the pile, while the other acts along its axial direction. The normal component induces a bending moment along the length of the pile. However, during tunnel excavation adjacent to the battered pile, additional bending moments can be induced in the pile. Fig. 10 compares the induced bending moment along the pile battered after completion of tunnelling in cases of S, T and B. A positive bending moment means that compressive stress was induced along the pile shaft facing the tunnel. In case of S, the positive bending moment is induced at the lower portion of the pile ($0.3 \leq Z/L_p \leq 0.7$). This is because of the combined effects of stress release caused by tunnelling (see Fig. 9) and the normal component of the working load to the battered pile. Since the head of the pile is free to move, there is negligible bending moment induced at the pile head.

The maximum bending moment of magnitude 370 kNm is induced at Z/L_p =0.48. However, negative bending moment is induced at the lower portion of the pile ($0.7 \leq Z/L_p \leq 1.0$). This is attributable to the location of the tunnel which is on the opposite side of the batter of the pile. The tunnelling-induced soil movement towards the tunnel resulting from significant stress release and the normal component of the working load are acting on the pile in opposite direction.

In the contrast, minimal bending moment is induced along the length of the battered pile in case of T. The reason is ascribed to the location of the tunnel which is on the opposite of the batter of the pile. The normal component of the vertical load and the tunnelling-induced ground movement have opposing effects, resulting in minimal bending moment. When the tunnel is excavated below the pile toes in case of B, positive bending moment is induced along the upper portion of the pile. However, the lower part of the pile experiences negative bending moment at the lower portion of the piles ($0.65 \leq Z/L_p \leq 0.77$). This is because the tunnel is excavated below the pile toe, the ground movement due to tunnelling is in vertical direction in the pile region (see Fig. 7). The maximum bending moment of 162 kNm occurs at Z/L_p=0.5.

4. Conclusions

The paper examines the settlements and load changes that occur in a battered pile due to an adjacent tunnel excavation. This study also includes parametric analyses to investigate the impact of different tunnel depths in relation to the pile length. Based on the results presented, the following conclusions can be drawn:

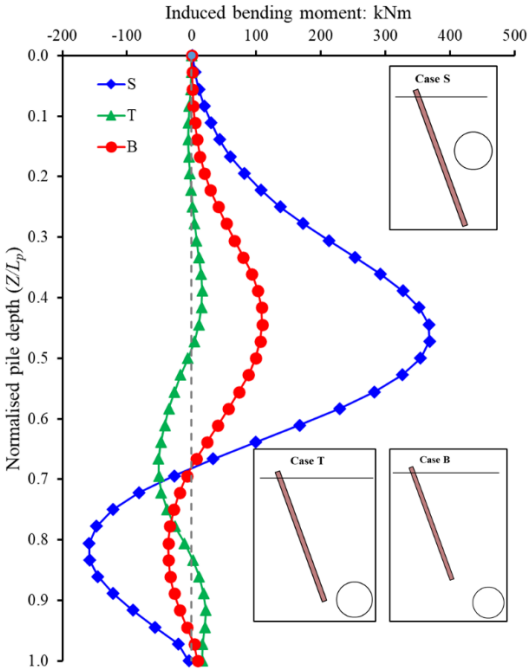

Fig. 10 Induced bending moment in the battered pile on completion of tunnel

a) The settlement and load transfer mechanisms along the battered pile as a result of tunnelling are highly dependent on the length of the pile. The largest settlement of the battered pile is induced in case of T. This is due to significant stress relief affecting the lower part of the pile, including the pile toe, as a result of tunnelling near the pile toe in case of T.
b) The largest pile deflection is caused by tunnelling next to the pile toe. This is because of the coupled effects of ground movement due to tunnelling-induced stress release and the normal component of the vertical working load on the pile head. The deflection of -2.96%d_p and -0.97%d_p were induced at the pile toe due to tunnelling in cases of T and B, respectively.
c) The battered pile is subjected to "dragload" due to negative skin friction mobilization due to tunnel excavation in cases of S. This occurs because the shaft of the battered pile experiences stress release due to tunnelling. Because the battered piles are installed at an angle, the surrounding soil settles more than the pile, causing it to be pulled downward and resulting in negative shaft resistance along the battered pile.
d) The battered pile is vulnerable in terms of induced bending moment when tunnelling is carried out near pile shaft in case of S. However, the magnitude of induced bending moment is minimal induced in case of B.

Acknowledgments

The authors would like to acknowledge the financial support provided by Quaid-e-Awam University of Engineering, Science & Technology, Sindh and Pakistan.

Conflicts of Interest

The authors declare that they have no conflicts of interest.

References

Al-Tabbaa, A. (1987), Permeability and stress-strain response of Speswhite Kaolin, PhD thesis. UK, University of Cambridge.

Abrams, A.J. (2007), Earth pressure balance (EPB) tunneling induced settlements in the Tren Urbano Project, Rio Piedras, Puerto Rico MEng thesis. Massachusetts Institute of Technology.

Benz, T. (2007), Small-strain stiffness and its numerical consequences, PhD thesis. Universitat Stuttgart.

Bharathi, M., Dubey, R.N. and Shukla, S.K. (2022), "Numerical simulation of the dynamic response of batter piles and pile groups", *Bul. Earthq. Eng.*, **20**(7), 3239-3263. https://doi.org/10.1007/s10518-022-01362-7.

Boonsiri, I. and Takemura, J. (2015), "Observation of ground movement with existing pile groups due to tunneling in sand using centrifuge modelling", *Geotech. Geol. Eng.*, **33**, 621-640. https://doi.org/10.1007/s10706-015-9845-0.

Boonyarak, T., Phisitkul, K., Ng, C.W.W., Teparaksa, W. and Aye, Z.Z. (2014), "Observed ground and pile group responses due to tunneling in Bangkok stiff clay", *Can.Geotech. J.*, **51**(5), 479-495. https://doi.org/10.1139/cgj-2013-0082.

Cheng, C.Y., Dasari, G.R., Chow, Y.K. and Leung, C.F. (2007), "Finite element analysis of tunnel-soil-pile interaction using displacement controlled model", *Tunn. Undergr. Sp. Tech.*, **22**(4), 450-466. https://doi.org/10.1016/j.tust.2006.08.002.

Coutts, D.R. and Wang, J. (2000), "Monitoring of reinforced concrete piles under horizontal and vertical loads", *Proceeding of the International Conference on Tunnels and Underground Structures*, Singapore.

Ding, Z., Wei, X.J. and Wei, G. (2017), "Prediction methods on tunnel-excavation induced surface settlement around adjacent

building", *Geomech. Eng.*, **12**(2), 185-195. https://doi.org/10.12989/gae.2017.12.2.185.

Franza, A. and Marshall, A.M. (2018), "Centrifuge modeling study of the response of piled structures to tunneling", *J. Geotech. Geoenviron. Eng*., **144**(2), 04017109. https://doi.org/10.1061/(ASCE)GT.1943-5606.000175.

Forth, R.A. and Thorley, C.B.B. (1996), "Hong Kong Island line predictions and performance", *Proceedings of the International Symposium on Geotechnical Aspects of Underground Construction in Soft Ground*, London. Balkema, Rotterdam, The Netherlands.

Gasparre, A. (2005), "Advanced laboratory characterisation of London Clay", Ph.D. thesis, Dept. of Civil and Environmental Engineering, Univ. of London.

Hibbitt, Karlsson, Sorensen. (2015), Abaqus user's manual, version 6.14-2. Providence, RI, USA: Hibbitt, Karlsson & Sorensen Inc.

Huang, M., Zhang, C. and Li, Z.A. (2009), "A simplified analysis method for the influence of tunnelling on grouped piles", *Tunn. Undergr. Sp. Tech*., **24**(4), 410-422. https://doi.org/10.1016/j.tust.2008.11.005.

Hong, Y., Soomro, M.A. and Ng, C.W.W. (2015), "Settlement and load transfer mechanism of pile group due to side-by-side twin tunneling", *Comput. Geotech*., **64**, 105-119. https://doi.org/10.1016/j.compgeo.2014.10.007.

Jamil, I. and Ahmad, I. (2019), "Bending moments in raft of a piled raft system using Winkler analysis", *Geomech. Eng.*, **18**(1), 41-48. https://doi.org/10.12989/gae.2019.18.1.041.

Indraratna, B., Balasubramaniam, A.S., Phamvan, P. and Wong, Y.K. (1992), "Development of negative skin friction on driven piles in soft Bangkok clay", *Can. Geotech. J*., **29**, 393-404. https://doi.org/10.1139/t92-044.

ISSMFE (1985), Axial pile loading test - Part I: Static loading. ASTM 8, 79-80.

Jacobsz, S.W., Bowers, K.H., Moss, N.A. and Zanardo, G. (2006), "The effects of tunnelling on piled structures on the CTRL. In: Geotechnical aspects of underground construction in soft ground", *Proceedings of the 5th international symposium TC28*. Amsterdam, the Netherlands, 15-17 June 2005.

Karira, H., Kumar, A., Ali, T.H., Mangnejo, D.A. and Mangi, N. (2022), "A parametric study of settlement and load transfer mechanism of piled raft due to adjacent excavation using 3D finite element analysis", *Geomech. Eng.*, **30**(2), 169-185. https://doi.org/10.12989/gae.2022.30.2.169.

Lee, C.J. and Chiang K.H. (2007), "Responses of single piles to tunnelling-induced soil movements in sandy ground", *Can. Geotech. J*., **44**, 1224-1241. https://doi.org/10.1139/T07-050.

Lee, C.J. (2012a), "Numerical analysis of the interface shear transfer mechanism of a single pile to tunnelling in weathered residual soil", *Comput. Geotech*., **42**, 193-203. https://doi.org/10.1016/j.compgeo.2012.01.009.

Lee, C.J. (2012b), "Three-dimensional numerical analyses of the response of a single pile and pile groups to tunnelling in weak weathered rock", *Tunn. Undergr. Sp. Tech*., **32**, 132-142. https://doi.org/10.1016/j.tust.2012.06.005.

Lee, G.T.K. and Ng, C.W.W. (2005), "The effects of advancing open face tunneling on an existing loaded pile", *J. Geotech. Geoenviron. Eng. – ASCE*, **131**(2), 193-201. https://doi.org/10.1061/(ASCE)1090-0241(2005)131:2(193).

Lee, C.J. (2013), "Numerical analysis of pile response to open face tunnelling in stiff clay", *Comput. Geotech*., **51**, 116-127. https://doi.org/10.1016/j.compgeo.2013.02.007.

Lee, S.W. (2019), "Experimental study on effect of underground excavation distance on the behavior of retaining wall", *Geomech. Eng.*, **17**(5), 413-420. https://doi.org/10.12989/gae.2019.17.5.413.

Li, H., Liu, S., Yan, X., Gu, W. and Tong, L. (2021), "Effect of loading sequence on lateral soil-pile interaction due to excavation", *Comput. Geotech*., **134**, 104134. https://doi.org/10.1016/j.compgeo.2021.104134.

Li, H., Liu, S. and Tong, L. (2022), "A numerical interpretation of the soil-pile interaction for the pile adjacent to an excavation in clay", *Tunn. Undergr. Sp. Tech*., **121**, 104344. https://doi.org/10.1016/j.tust.2021.104344.

Loganathan, N., Poulos, H.G. and Stewart, D.P. (2000), "Centrifuge model testing of tunnelling-induced ground and pile deformations", *Géotechnique*, **50**, 283-294. https://doi.org/10.1680/geot.2000.50.3.283.

Loganathan, N., Poulos, H.G. and Xu, K.J. (2001), "Ground and pile group responses due to tunneling", *Soils Found*., **41**(1), 57-67. https://doi.org/10.3208/sandf.41.57.

Liu, M., Meng, F., Chen, R., Cheng, H. and Li, Z. (2023), "Numerical study on the lateral soil arching effect and associated tunnel responses behind braced excavation in clayey ground", *Transport. Geotech*., **40**, 100970. https://doi.org/10.1016/j.trgeo.2023.100970.

Lu, H., Shi, J., Ng, C.W.W. and Lv, Y. (2020), "Three-dimensional centrifuge modeling of the influence of side-by-side twin tunneling on a piled raft", *Tunn. Undergr. Sp. Tech*., **103**, 103486. https://doi.org/10.1016/j.tust.2020.103486.

Mair, R.J. and Taylor, R.N. (1997), "Bored tunnelling in the urban environment. State-of-the-art Report and Theme Lecture", *Proceedings of the 14th International Conference on Soil Mechanics and Foundation Engineering*, Hamburg, Balkema.

Marshall, A.M. and Mair, R.J. (2011), "Tunneling beneath driven or jacked end-bearing piles in sand", *Can. Geotech. J*., **48**(12), 1757-1771. https://doi.org/10.1139/t11-067.

Marshall, A.M. (2012), "Tunnel-pile interaction analysis using cavity expansion methods", *J. Geotech. Gooenviron. Eng*., **138**(10), 1237-1246. https://doi.org/10.1061/(ASCE)GT.1943-5606.0000709.

Mašín, D. (2005), "A hypoplastic constitutive model for clays", *Int. J. Numer. Anal. Meth. Geomech*., **29**(4), 311-336. https://doi.org/10.1002/nag.416.

Mašín, D. and Herle, I. (2005), "State boundary surface of a hypoplastic model for clays", *Comput. Geotech*., **32**(6), 400-410. https://doi.org/10.1016/j.compgeo.2005.09.001.

Mayne, P. and Kulhawy, F. (1982), "K0-OCR relationships in soils", *J. Geotech. Eng. - ASCE*, **108**(6), 851-872.

Meguid, M.A., Saada, O., Nunes, M.A. and Mattar, J. (2008), "Physical modeling of tunnels in soft ground: a review", *Tunn. Undergr. Sp. Tech*., **23**(2),185-198. https://doi.org/10.1016/j.tust.2007.02.003.

Mroueh, H. and Shahrour, I. (2002), "Three-dimensional finite element analysis of the interaction between tunnelling and pile foundations", *Int. J. Numer. Anal. Method. Geomech*., **26**(3), 217-230. https://doi.org/10.1002/nag.194.

Mu, L., Huang, M., Roodi, G.H. and Shi, Z. (2021), "Allowable wall deflection of braced excavation adjacent to pile-supported buildings", *Geomech. Eng*., **26**(2), 161-173. https://doi.org/10.12989/gae.2021.26.2.161.

Ng, C.W.W., Lu, H. and Peng, S.Y. (2013), "Three-dimensional centrifuge modelling of effects of twin tunnelling on as existing pile", *Tunn. Undergr. Sp. Tech*., **35**, 189-199. https://doi.org/10.1016/j.tust.2012.07.008.

Ng, C.W.W. nad Lu, H, (2013), "Effects of construction sequence of twin tunnelling at different depth on a single pile", *Can. Geotech. J*., **51**(2), 173-183. https://doi.org/10.1139/cgj-2012-0452.

Ng, C.W.W., Soomro, M.A. and Hong, Y. (2014), "Three-dimensional centrifuge modelling of pile group responses to side-by-side twin tunneling", *Tunn. Undergr. Sp. Tech*., **43**, 350-361. https://doi.org/10.1016/j.tust.2014.05.002.

Ng, C.W.W., Hong, Y. and Soomro, M.A. (2015), "Effects of piggyback twin tunnelling on a pile group: 3D centrifuge tests and numerical modelling", *Géotechnique*, **65**(1), 38-51. https://doi.org/10.1680/geot.14.P.105.

Niemunis, A. and Herle, I. (1997), "Hypoplastic model for cohesionless soils with elastic strain range", *Mech. Cohesive-Frict. Mater.*, **2**(4), 279-299. https://doi.org/10.1002/(SICI)10991484(199710)2:4<279::AID-CFM29>3.0.CO;2-8.

Pang, C.H., Yong, K.Y. and Chow, Y.K. (2005), Three dimensional numerical simulation of tunnel advancement on adjacent pile foundation. Underground Space Use: Analysis of the Past and Lessons for the Future (Eds., Y. Erdem and T. Solak), 1141-1147. London: Taylor and Francis.

Parry, R.H.G. and Nadarajah, V. (1974), "Observations on laboratory prepared, lightly overconsolidated specimens of kaolin", *Géotechnique*, **24**(3) 345-358. https://doi.org/10.1680/geot.1974.24.3.345.

Powrie, W. (1986), The behavior of diaphragm walls in clay, Ph.D. thesis. University of Cambridge, UK.

Poulos, H.G. (2001), "Piled raft foundations: Design and applications", *Géotechnique*, **51**(2), 95-113. https://doi.org/10.1680/geot.2001.51.2.95.

Qian, J., Tong, Y., Mu, L., Lu, Q. and Zhao, H. (2020), "A displacement controlled method for evaluating ground settlement induced by excavation in clay", *Geomech. Eng.*, **20**(4), 275-285. https://doi.org/10.12989/gae.2020.20.4.275.

Selemetas, D. (2005), The response of full-scale piles and pile structures to tunneling. Ph.D. thesis, Cambridge University.

Shi, J., Fu, Z. and Guo, W. (2019a), "Investigation of geometric effects on three-dimensional tunnel deformation mechanisms due to basement excavation", *Comput. Geotech.*, **106**, 108-116. https://doi.org/10.1016/j.compgeo.2018.10.019.

Shi, J., Wei, J., Ng, C.W.W. and Lu, H. (2019b), "Stress transfer mechanisms and settlement of a floating pile due to adjacent multi-propped deep excavation in dry sand", *Comput. Geotech.*, **116**, 103216. https://doi.org/10.1016/j.compgeo.2019.103216.

Shi, J., Ding, C., Ng, C.W.W., Lu, H. and Chen, L. (2020), "Effects of overconsolidation ratio on tunnel responses due to overlying basement excavation in clay", *Tunn. Undergr. Sp. Tech.*, **97**, 103247. https://doi.org/10.1016/j.tust.2019.103247.

Shi, J., Wang, J., Chen, Y., Shi, C., Lu, H., Ma, S. and Fan, Y. (2023), "Physical modeling of the influence of tunnel active face instability on existing pipelines", *Tunn. Undergr. Sp. Tech.*, **140**, 105281. https://doi.org/10.1016/j.tust.2023.105281.

Shirlaw, J.N., Ong, J.C.W., Rosser, H.B., Tan, C.G., Osborne, N.H. and Heslop, P.E. (2003), "Local settlements and sinkholes due to EPB tunneling", *Geotech. Eng.*, **156**(4), 193-211. https://doi.org/10.1680/geng.2003.156.4.193.

Soomro, M.A., Hong, Y., Ng, C.W.W., Lu, H. and Peng, S.Y. (2015), "Load transfer mechanism in pile group due to single tunnel advancement in stiff clay", *Tunn. Undergr. Sp. Tech.*, **45**, 63-72. https://doi.org/10.1016/j.tust.2014.08.001.

Soomro, M.A., Ng, C.W.W., Liu, H. and Memon, N.A. (2017), "Pile responses to side-by-side twin tunnelling in stiff clay: Effects of different tunnel depths relative to pile", *Comput. Geotech.*, **84**, 101-116. https://doi.org/10.1016/j.compgeo.2016.11.011.

Soomro, M.A., Kumar, M., Xiong, H., Mangnejo, D.A. and Mangi, N. (2020), "Investigation of effects of different construction sequences on settlement and load transfer mechanism of single pile due to twin stacked tunneling", *Tunn. Undergr. Sp. Tech.*, **96**, 103171. https://doi.org/10.1016/j.tust.2019.103171.

Soomro, M.A., Mangi, N., Memon, A.H. and Mangnejo, D.A. (2022), "Responses of high-rise building resting on piled raft to adjacent tunnel at different depths relative to piles", *Geomech. Eng.*, **29**(1), 25-40. https://doi.org/10.12989/gae.2022.29.1.025.

Tsubakihara, Y. and Kishida, H. (1993), "Frictional behaviour between normally consolidated clay and steel by two direct shear type apparatuses", *Soils Found.*, **33**(2), 1-13. https://doi.org/10.3208/sandf1972.33.2_1.

Ye, X.W., Zhang, X.L., Zhang, H.Q., Ding, Y. and Chen, Y.M. (2023), "Prediction of lining upward movement during shield tunneling using machine learning algorithms and field monitoring data", *Transport. Geotech.*, **41**, 101002. https://doi.org/10.1016/j.trgeo.2023.101002.

Zhang, R.J., Zheng, J.J., Zhang, L.M. and Pu, H.F. (2011), "An analysis method for the influence of tunneling on adjacent loaded pile groups with rigid elevated caps", *Int. J. Numer. Anal. Method. Geomech.*, **35**(18), 1949-1971. https://doi.org/10.1002/nag.989.

GC